Inorg. Chem. **2004**, *43*, 8336–8345

Synthesis, Structure, and Solution Dynamics of UO_2^{2+}–Hydroxy Ketone Compounds $[UO_2(ma)_2(H_2O)]$ and $[UO_2(dpp)(Hdpp)_2(H_2O)]ClO_4$ [ma = 3-Hydroxy-2-methyl-4-pyrone, Hdpp = 3-Hydroxy-1,2-dimethyl-4(1*H*)-pyridone]

Chryssoula Drouza,[†] Volker Gramlich,[‡] Michael P. Sigalas,*[,§] Ioannis Pashalidis,[†] and Anastasios D. Keramidas*[,†]

Department of Chemistry, University of Cyprus, 1678 Nicosia, Cyprus, Laboratory of Crystallography, NOG62 CH-8092 Zurich, Switzerland, and Chemistry, Aristotle University of Thessaloniki, 54006 Thessaloniki, Greece

Received June 26, 2004

Reaction of $[UO_2(NO_3)_2]$ with the hydroxy ketones 3-hydroxy-2-methyl-4-pyrone (Hma) and 3-hydroxy-1,2-dimethyl-4(1*H*)-pyridone (Hdpp) in aqueous acidic solutions (pH ∼ 3) yields the compounds $[UO_2(ma)_2(H_2O)]\cdot H_2O$ (**1**·H_2O) and $[UO_2(dpp)(Hdpp)_2(H_2O)]ClO_4$ (**2**), respectively. X-ray diffraction shows that the geometry around the metal ion in both complexes is pentagonal bipyramid. Uranium ion in the crystal structure of **1** were found to be ligated with two chelate ma^- groups and one unidentate H_2O molecule (**C** coordination mode) at the equatorial plane, while in **2** with two single-bonded Hdpp there were one chelate dpp^- and one H_2O molecule (**P** coordination mode). Crystal data (Mo Kα; 293(2) K) are as follows: (**1**) monoclinic space group *C*2/*c*, $a = 14.561(7)$ Å, $b = 14.871(9)$ Å, $c = 7.250(4)$ Å, $\beta = 95.40(4)°$, $Z = 4$; (**2**) monoclinic space group $P2_1/c$, $a = 19.080(2)$ Å, $b = 9.834(1)$ Å, $c = 15.156(2)$ Å, $\beta = 104.62(1)°$, $Z = 4$. ^1H NMR measurements indicate that complex **2** retains its structure in CD_3CN solution; however, in DMSO-d_6 both complexes adopt the **C** structure. Line-shape analysis for the ^1H NMR peaks of **2** at various temperatures shows a fast intramolecular exchange process between the chelate dpp^- and one of the single bonded Hdpp ligands and one slower exchange between all three ligands. The activation parameters and the decrease of the exchange rate by replacing unidentate ligand with DMSO indicate the dissociation of the unidentate ligand as the rate-determining step for the former exchange. Density functional calculations (DFT) support this mechanism and give a quantitative interpretation of the electronic structure of the two ligands and the geometries adopted by the complexes.

Introduction

Uranium contamination in soil and groundwater from the increased handling of uranium in the nuclear cycle worldwide and the release of the element from spent nuclear fuel repositories as well as the military use of depleted uranium poses a risk to both human health and environment. Although the effects on health of humans from environmental exposure to uranium are beginning to be documented, the chemical toxicity of uranium is still poorly understood.[1,2] There has been considerable interest in the design of selective UO_2^{2+} chelators suitable for uranium removal from soil, groundwater, and/or human bodies.[3,4] Organic bidentate ligands containing hard oxygen donor atoms have the ability to match the equatorial 5-coordinate environment of the UO_2^{2+} cation, and so far, they have been presented as good candidates for selective binding with uranium.[3−8] In particular, catechols, β-diketones, and hydroxy ketones such as 4,5-dihydroxy-

* Authors to whom correspondence should be addressed. E-mail: akeramid@ucy.ac.cy (A.D.K.). Fax: (357)22892801 (A.D.K.); sigalas@chem.auth.gr (M.P.S.).
[†] University of Cyprus.
[‡] Laboratory of Crystallography.
[§] Aristotle University of Thessaloniki.

(1) Carriere, M.; Avoscan, L.; Collins, R.; Carrot, F.; Khodja, H.; Ansoborlo, E.; Gouget, B. *Chem. Res. Toxicol.* **2004**, *17*, 446.
(2) Yazzie, M.; Gamble, S. L.; Civitello, E. R.; Stearns, D. M. *Chem. Res. Toxicol.* **2003**, *16*, 524.
(3) Gorden, A. E. V.; Xu, J.; Raymond, K. N.; Durbin, P. *Chem. Rev.* **2003**, *103*, 4207−4282.
(4) Xu, J.; Raymond, K. N. *Inorg. Chem.* **1999**, *38*, 308−315.
(5) Kannan, S.; Venugopal, V.; Pillai, M. R. A.; Droege, P. A.; Barnes, C. L. *Polyhedron* **1996**, *15*, 97−101.
(6) Kannan, S.; Ferguson, G. *Inorg. Chem.* **1997**, *36*, 1724−1725.

10.1021/ic049167+ CCC: $27.50
Published on Web 11/19/2004

Chart 1. Coordination Mode of Hydroxy Ketones in UO_2^{2+} Complexes (X = O or N)

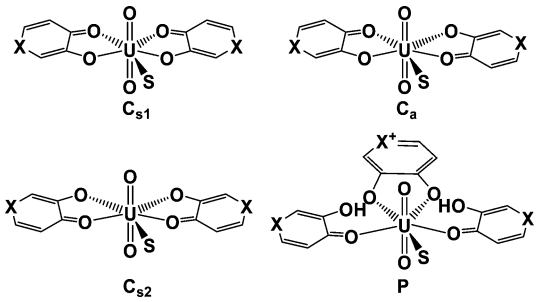

3,5-benzenedisulfonate (Tiron), 1-hydroxy-2(*1H*)-pyridinone, and 1-methyl-3-hydroxy-2(*1H*)-pyridone (Me-2,3-HOPO) have demonstrated high efficiency for decorporation of U^{VI} from body and kidney in animals.[9−14] In addition, hydroxy ketone ligands have the advantage of low toxicity. For example, maltol (Hma) has been already approved as a food additive and is sold in health food stores, while hydroxypyridones have been successfully utilized as oral potent sequestering agents for hard metal ions, such as Fe^{III}, from the human body.[15]

Detailed study of the solid state and solution chemistry of uranium is essential for understanding the in vivo chelation efficacy of these ligands and the mechanisms in the processing of nuclear waste and materials. The structures of solid UO_2^{2+}−diketonates and −hydroxy ketonates have revealed the coordination sphere of metal ion in the equatorial plane to be defined from the donor atoms of two chelate bidentate ligands as well as the donor atom of one-unidentate ligand (**C** coordination mode, Chart 1).[3−6,16−18] However, in solution the composition of these complexes may vary, including compounds containing one, two, or three bidentate ligands, as evidenced by equilibrium analytical methods and NMR spectroscopy.[7,19,20]

Herein, we report the synthesis and physicochemical and structural characterization of two novel uranyl complexes, namely $[UO_2(ma)_2(H_2O)]\cdot H_2O$ (**1**·H_2O) and $[UO_2(dpp)(Hdpp)_2(H_2O)]ClO_4$ (**2**). The experimental data are quantitatively interpreted by density functional calculations (DFT). Complex **2** shows a unique structure with one chelate dpp^- and two single-bonded Hdpp ligands (**P** coordination mode, Chart 1) coordinated at the equatorial plane of UO_2^{2+}. This compound is a rare example of a fully characterized uranyl compound containing three bidentate ligands coordinated to a uranium ion.[21] The ^1H NMR spectra of **1** and **2** in solution reveal that the coordination mode of the hydroxy ketones is solvent dependent. This may be related to the sulfoxide (e.g. DMSO) induced enhancement of the extraction−separation of uranyl cation by β-diketones in acidic media.[5] Variable-temperature ^1H NMR spectroscopy shows that the three ligands in complex **2** are exchanging through two exchange processes, a fast intramolecular exchange between the chelate and one of the single bonded ligands and a slow exchange between all three hydroxy ketonates. The possible mechanisms for these two exchange processes are discussed in the light of these ^1H NMR studies and density functional calculations as well.

Experimental Section

Materials. Reagent grade uranyl nitrate hexahydrate and uranyl acetate dihydrate were purchased from Merck. 3-Hydroxy-2-methyl-4-pyrone (Hma), 3-hydroxy-1,2-dimethyl-4(1*H*)-pyridone (Hdpp), and sodium perchlorate were reagent grade and were obtained from Aldrich. All chemicals were used without further purification. IR spectra were recorded on a Jasco FT-IR 460 plus spectrometer in KBr pellets. Microanalyses were performed by Desert Analytics, Tucson, AR. (**Caution!** *Perchlorate salts are potentially explosive. All compounds containing perchlorate should be handled with great care and in small amounts.*)

Preparation of $[UO_2(ma)_2(H_2O)]\cdot H_2O$ (1·H_2O). Orange crystals of **1**·H_2O were obtained in 81% yield by layering a methanol (5 mL) solution of Hma (0.15 g, 1.2 mmol) over an uranyl aqueous solution (5 mL) of $UO_2(NO_3)_2\cdot 6H_2O$ (0.20 g, 0.40 mmol). ^1H NMR (δ; DMSO-d_6) at 293 K: 8.43 (2H, d, C4H), 6.92 (2H, d, C5H), 2.65 (6H, s, C6H). ^{13}C NMR (δ; DMSO-d_6) at 293 K: 185.8 (C1), 159.2 (C2), 157.2 (C4), 155.7 (C3), 113.8 (C5), 15.02 (C6). The numbering is according to Figure 1A. The infrared spectrum of **1**·H_2O exhibited bands at 1560 (s, C═O), 1209 (s, C−O), and 926 cm^{-1} (s, U═O). Anal. Calcd for $C_{12}H_{14}O_{10}U$: C, 25.91; H, 2.54, Found: C, 25.70; H, 2.66.

Preparation of $[UO_2(dpp)(Hdpp)_2(H_2O)]ClO_4$ (2). Orange crystals of **2** were obtained in 80% yield by slow evaporation, at room temperature, of an aqueous solution (100 mL) containing 0.1 M $NaClO_4$, $UO_2(NO_3)_2\cdot 6H_2O$ (0.125 g, 0.250 mmol), and Hdpp (0.104 g, 0.750 mmol) at pH = 3.0. ^1H NMR at 224 K (δ; CD_3CN): 12.3 (1H, s, O4H), 12.0 (1H, s, O6H), 7.83 (1H, d, C18H), 7.85 (1H, d, C11H), 7.67 (1H, d, C4H), 7.22 (2H, d, C12H, C19H), 6.68 (1H, d, C5H), 3.82 (9H, s, C7H, C14H, C20H), 2.64 (3H, s, C6H), 2.47 (3H, s, C13H), 2.44 (3H, s, C21H). The numbering is according to Figure 1B. The infrared spectrum of **2** exhibited the following peaks: 1554 (s, C═O), 1292 (s, C−O), 883 cm^{-1} (s, U═O). Anal. Calcd for $C_{21}H_{28}ClN_3O_{13}U$: C, 31.37; H, 3.51; N, 5.23. Found: C, 31.17; H, 3.58; N, 5.06.

X-ray Structure Determination. Crystals suitable for X-ray diffraction study were obtained directly from the reaction mixtures

(7) Sylwester, E. R.; Allen, P. G.; Dharmawardana, U. R.; Sutton, M. *Inorg. Chem.* **2001**, *40*, 2835−2841.
(8) Jacopin, C.; Sawicki, M.; Plancque, G.; Doizi, D.; Taran, F.; Ansoborlo, E.; Amekraz, B.; Moulin, C. *Inorg. Chem.* **2003**, *42*, 5015.
(9) Durbin, P. W.; Kullgren, B.; Ebbe, S. N.; Xu, J. D.; Raymond, K. N. *Health Phys.* **2000**, *78*, 511.
(10) Durbin, P. W.; Kullgren, B.; Xu, J. D.; Raymond, K. N. *Health Phys.* **1997**, *72*, 865.
(11) Durbin, P. W.; Kullgren, B.; Xu, J. D.; Raymond, K. N. *Radiat. Prot. Dosim.* **1994**, *53*, 304.
(12) Domingo, J. L.; Ortega, A.; LIobet, J. M.; Paternain, J. L.; Corbella, J. *Res. Commun. Pathol. Pharmacol.* **1989**, *64*, 161.
(13) Stradling, G. N.; Gray, S. A.; Moody, J. C.; Ellender, M. *Hum. Exp. Toxicol.* **1991**, *10*, 195.
(14) Stradling, G. N. *J. Alloys Compd.* **1998**, *271*−*273*, 72.
(15) Tilbrook, G. S.; Hider, R. C. Iron Chelators for clinical use. In *Metal Irons in Biological Systems. Vol. 35: Iron Transport and Storage in Microorganisms, Plants and Animals*; Sigel, A., Sigel, H., Eds.; Marcel Dekker: New York, 1998; pp 691−730.
(16) Bokolo, K.; Courtois, A.; Delpuech, J.-J.; Elkaim, E.; Protas, J.; Rinaldi, D.; Rodehuser, L.; Rubini, P. *J. Am. Chem. Soc.* **1984**, *106*, 6333.
(17) Lintvedt, R. L.; Heeg, M. J.; Ahmad, N.; Glick, M. D. *Inorg. Chem.* **1982**, *21*, 2350.
(18) Kramer, G. M.; Dines, M. B.; Hall, R. B.; Kaldor, A.; Jacobson, A. J.; Scanlon, J. C. *Inorg. Chem.* **1980**, *19*, 1340.
(19) Bokolo, K.; Delpuech, J.-J.; Rodehuser, L.; Rubini, P. R. *Inorg. Chem.* **1981**, *20*, 992.
(20) Chiacchierini, E.; Havel, J.; Sommer, L. *Collect. Czech. Chem. Commun.* **1968**, *33*, 4215.
(21) Berthet, J.-C.; Nierlich, M.; Ephritikhine, M. *Chem. Commun.* **2003**, 1660.

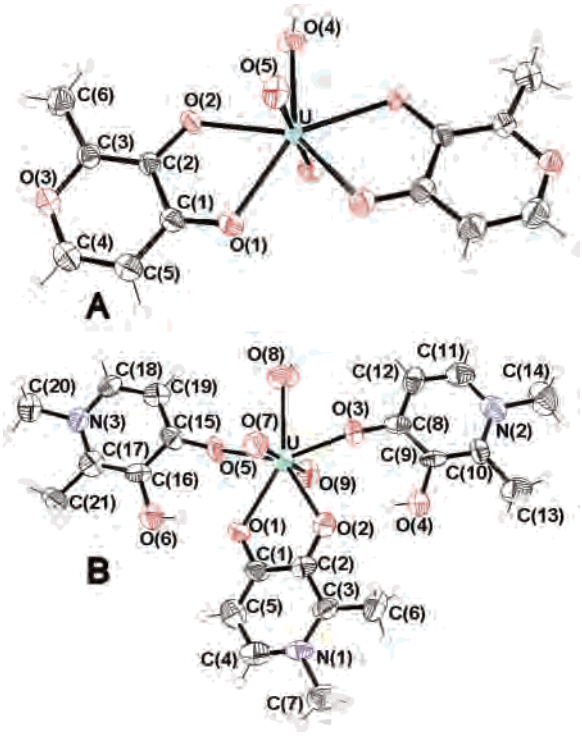

Figure 1. ORTEP drawing of (A) **1**·MeOH and (B) **2** at 50% probability ellipsoids giving atomic numbering. For clarity, the hydrogen atoms of **2** and cocrystallized molecules are omitted.

Table 1. Crystal Data and Structure Refinement for **1** and **2**

param	**1**	**2**
empirical formula	$C_{13}H_{16}O_{10}U$	$C_{21}H_{28}ClN_3O_{13}U$
cryst size (mm)	0.1 × 0.1 × 0.1	0.24 × 0.017 × 0.007
fw	570.29	803.94
temp (K)	293(2)	293(2)
wavelength (Å)	0.710 73	0.710 73
cryst syst	monoclinic	monoclinic
space group	*C*2/*c*	$P2_1/c$
a (Å)	14.561(7)	19.080(2)
b (Å)	14.871(9)	9.835(1)
c (Å)	7.250(4)	15.156(2)
β (deg)	95.50(4)	104.62(1)
V (Å^3)	1563(2)	2751.7(4)
Z	4	4
ρ_{calcd} (Mg/m^3)	2.424	1.921
abs coeff (mm^{-1})	10.44	6.03
θ range for data collcn (deg)	1.96−20.03	3.91−20.04
index ranges	$0 \le h \le 14$, $0 \le k \le 14$, $-6 \le l \le 6$	$-18 \le h \le 18$, $-9 \le k \le 9$, $-14 \le l \le 14$
no. of obsd reflcns	678	24 393
no. of indpndt reflcns	733	2571
data/params	5.8	7.18
max/min $\Delta\rho$ (e Å^{-3})	1.033, −0.692	0.527, −0.434
R, wR (obsd data)[a]	0.0222, 0.0531	0.0587, 0.0833
R, wR (all data)[a]	0.0239, 0.0533	0.0887, 0.0914

[a] Refinement method, full-matrix least squares on F^2.

of both complexes. The X-ray structure showed one molecule of CH_3OH to be cocrystallized with **1**. The intensity data for **1** for these studies were collected on a Syntex P21 4-cycle diffractometer and data for **2** on an Oxford XCalibur using Mo Kα (λ = 0.7107 Å) radiation. Experimental data for this study are listed in Table 1. Each structure was solved by direct methods using program SHELX-86[22] and refined by full-matrix least-squares techniques.[23]

The positions of the hydrogen atoms of **1** and **2** were calculated from stereochemical considerations and kept fixed isotropic during refinement. CCDC reference numbers are 207139 (**1**·CH_3OH) and 207140 (**2**).

NMR Spectroscopy. All NMR samples were prepared from crystalline compounds in DMSO-d_6 or in CD_3CN at room temperature immediately before NMR spectrometric determinations. All samples used to NMR measurements were prepared in triplicate, typically at concentrations of 1−30 mg/mL complex. NMR spectra were recorded on a Bruker Avance 300 spectrometer at 300 MHz for ^{1}H and 75.4 MHz for ^{13}C NMR. The 1D ^{1}H and ^{13}C NMR spectra were acquired with a 6000 and 19 000 Hz spectral window, respectively, a 30° pulse width, and a 2.0 s relaxation delay.

T_1 measurements were obtained by using the inversion recovery method. The magnitude 2D ^{1}H COSY-45 experiments (pulse sequence 90°−t_1−45°) were acquired using 256 increments (each consisting of 32 scans) covering the full spectrum (10 ppm in both dimensions). The standard NOESY pulse sequence (90°−t_1−90°−t_m−90°) was used in the 2D ^{1}H EXSY−NOESY measurements. These spectra were acquired using 256 increments of size 2 K (with 40 scans each) covering the full spectrum (10 ppm in both dimensions). The delay time used in the 2D spectra was based on the measured T_1 values and was 4.5 s. Variable mixing times ranging from 0.25 to 0.90 s were used. The chemical shifts were referenced to TMS.

The variable-temperature NMR experiments required that the NMR spectrometer be calibrated to within ±1 °C using a 4% CH_3OH/CD_3OD standard for the low temperatures and 80% ethylene glycol/DMSO-d_6 standard for the high temperatures. The probe temperature was allowed to equilibrate for 10 min prior to final magnetic homogeneity optimization on the ^{1}H FID. For each sample the temperature was varied in both directions, and in each case superimposable spectra were obtained. The values of the reaction rates of the exchange systems were calculated by the trial and error matching of the experimental spectrum measured at the specific temperature with a series of theoretical spectra calculated for different reaction rates. Theoretical line shapes were computed by using the gNMR program.[24] Line widths, chemical shifts, and spin−spin coupling constants used in the fast exchange were obtained from the stop exchange values, in the temperature range 224−233 K. The rate constants were fitted as a function of 1/*T* according to the Eyring plot [$k = (k_BT/h)\exp(-\Delta G^{\ddagger}/RT)$]. Activation parameters $\Delta G^{\ddagger}$, $\Delta H^{\ddagger}$, and $\Delta S^{\ddagger}$ were obtained from the least-squares fit of log(*k*/*T*) vs 1/*T* plots. All errors are random errors estimated at the 95% confidence level.

Computational Details. The electronic structure and geometry of the uranyl complexes were computed within the density functional theory. The hybrid B3LYP method was applied with Becke's three-parameter functional,[25] and the nonlocal correlation is provided by the LYP expression.[26] A significant reduction in the size of computations was achieved by replacing the core electron by a relativistic effective core potential (ECP). Previous studies[27−29] have shown that the accuracy of the energy consistent ECPs of

(22) Sheldrick, G. M. *SHELXS-86: Program for the Solution of Crystal Structure*; University of Gottingen: Gottingen, Germany, 1990.
(23) Sheldrick, G. M. *SHELXL-93: Program for the Refinement of Crystal Structure*; University of Gottingen: Gottingen, Germany, 1993.
(24) Budzelaar, H. M. P. *gNMR*, version 4.1.0; Cherwell Schientific Publishing: Oxford, U.K., 1999.
(25) Becke, A. D. *J. Chem. Phys.* **1993**, *98*, 5648.
(26) Lee, C.; Yang, W.; Parr, R. G. *Phys. Rev. B.* **1988**, *37*, 785.
(27) Vallet, V.; Maron, L.; Schimmelpfennig, B.; Leininger, T.; Teichteil, C.; Gropen, O.; Grenthe, I. *J. Phys. Chem.* **1999**, *103*, 9285.
(28) Vallet, V.; Schimmelpfennig, B.; Maron, L.; Teichteil, C.; Leininger, T.; Grenthe, I.; U., W. *Chem. Phys.* **1999**, *244*, 185.
(29) Vallet, V.; Wahlgren, U.; Schimmelpfennig, B.; Moll, H.; Szabo, Z.; Grenthe, I. *Inorg. Chem.* **2001**, *40*, 3516.

Stuttgart-type[30,31] is excellent; hence, we used these for both uranium and main group atoms, except for the hydrogen atoms, which were described by Dunning/Huzinaga valence double-ζ basis.[32] All the calculations have been done using models of the ligands, where the methyl substituents have been replaced by hydrogens. The geometry of all the species studied was optimized using gradient techniques under the symmetry constraints mentioned within the text. As the size of the molecules did not permitted frequency calculations and to ensure that the minima located are true local minima, each optimized structure has been slightly distorted and reoptimized using tight convergence in the optimization process. All of the calculations were performed using the Gaussian03 package.[33]

Results and Discussion

Synthesis of the Compounds. When water−methanol solutions of $[UO_2(NO_3)_2]$ are treated with 2 or 3 equiv of Hma, orange crystals of $[UO_2(ma)_2(H_2O)]\cdot H_2O$ (**1**·H_2O) are obtained. Using a 1:3 stoichiometry between $[UO_2(NO_3)_2]$ and Hdpp in aqueous or water methanol solutions allows for the isolation of a product of composition $[UO_2(dpp)(Hdpp)_2(H_2O)]NO_3$. Addition of $NaClO_4$ in the solution results in exchange of the NO_3^- counterion with ClO_4^- producing orange crystals of $[UO_2(dpp)(Hdpp)_2(H_2O)]ClO_4$ (**2**). Both complexes, **1** and **2**, are very soluble in DMSO and sparingly soluble in water, alcohols, and acetonitrile. The perchlorate salt of **2** was preferred for the NMR studies to the nitrate, because of its higher solubility in polar organic solvents. The solids and the solutions of these materials are stable at room temperature for long periods (over 1 month).

X-ray Crystallographic Results. The ORTEP structural plots for **1**·CH_3OH and **2** are presented in Figure 1. Crystallographic data and interatomic bond lengths and angles are provided in Tables 1 and 2, respectively.

The coordination environment of the uranium atom in **1** is a distorted pentagonal bipyramid with two oxo groups occupying the apical positions. Four oxygen atoms originated from two chelate ma^- ligands and one water oxygen atom define the equatorial plane of the pentagonal bipyramid of **1** ($\mathbf{C_{s1}}$ coordination mode, Chart 1). Both Hdpp and Hma could be considered as a resonance hybrid of two canonical forms, **I** and **II** (Scheme 1). The d(C−O_{ketone}) [C(1)−O(1), 1.281(10) Å] of the two chelate ma^- groups in **1** were found significantly shorter (∼0.06 Å) than the C−$O_{hydroxy}$ bonds [C(2)−O(2), 1.335(10) Å], indicating a double or partial double bond for the C−O_{ketone} (type **I** resonance form). The d[U−O(2)] [2.362(5) Å] in **1** is substantially shorter than d[U−O(1)] [2.429(13) Å] indicating the stronger preference of UO_2^{2+} for the hydroxy than the ketonic oxygen atom. In general, the binding mode of the organic ligands in the structure of complex **1** ($\mathbf{C_{s1}}$ mode) is similar to that found in other uranium(VI) complexes containing bidentate ligands, such as 2,5-diketones[5,6] and hydroxy ketones.[4] All these complexes contain two bidentate chelate ligands, and the U−O bond distances between the uranium atom and the ligand donor atoms are in the range of 2.30−2.45 Å. There is a single example of a bidentate hydroxy ketonate−uranyl complex, $[UO_2(Me\text{-}2,3\text{-}HOPO)_2(DMF)]$, which has been reported in the literature and characterized by crystallography, with the ligand in a $\mathbf{C_a}$ coordination mode (Chart 1).[4] The

Table 2. Selected Bond Lengths (Å) and Angles (deg) for **1**[a] and **2**

Bond Lengths for **1**			
U−O(1)	2.429(5)	U−O(2)	2.362(5)
U−O(4)	2.343(10)	U−O(5)	1.759(6)
U−O(1)$^{\#1}$	2.429(5)	U−O(2)$^{\#1}$	2.362(5)
U−O(5)$^{\#1}$	1.759(6)	C(2)−O(2)	1.335(10)
C(1)−O(1)	1.281(10)		
Bond Angles for **1**			
O(1)$^{\#1}$−U−O(1)	74.1(3)	O(2)$^{\#1}$−U−O(1)	140.4(2)
O(2)−U−O(1)	67.0(2)	O(4)−U−O(1)	142.96(14)
O(5)$^{\#1}$−U−O(1)	87.1(2)	O(2)$^{\#1}$−U−O(1)$^{\#1}$	67.0(2)
O(2)−U−O(1)$^{\#1}$	140.4(2)	O(4)−U−O(1)$^{\#1}$	142.96(14)
O(5)−U−O(1)$^{\#1}$	87.1(2)	O(5)$^{\#1}$−U−O(1)$^{\#1}$	94.4(2)
O(2)−U−O(2)$^{\#1}$	152.5(3)	O(4)−U−O(2)$^{\#1}$	76.23(13)
O(5)−U−O(2)$^{\#1}$	91.0(2)	O(5)$^{\#1}$−U−O(2)$^{\#1}$	88.6(2)
O(4)−U−O(2)	76.23(13)	O(5)−U−O(2)	88.6(2)
O(5)$^{\#1}$−U−O(2)	91.0(2)	O(5)−U−O(4)	89.0(2)
O(5)$^{\#1}$−U−O(4)	89.0(2)	O(5)$^{\#1}$−U−O(5)	178.1(4)
Bond Lengths for **2**			
U−O(1)	2.433 (10)	U−O(2)	2.384(12)
U−O(3)	2.273(9)	U−O(5)	2.281 (9)
U−O(7)	1.788(9)	U−O(8)	2.472(10)
U−O(9)	1.771(9)	C(1)−O(1)	1.334(17)
C(2)−O(2)	1.316(18)	C(15)−O(5)	1.297(17)
C(16)−O(6)	1.372(17)	C(9)−O(4)	1.366(16)
C(8)−O(3)	1.278(16)		
Bond Angles for **2**			
O(7)−U−O(9)	178.8(4)	O(7)−U−O(3)	88.3(4)
O(9)−U−O(3)	92.2(4)	O(7)−U−O(5)	91.2(4)
O(9)−U−O(5)	87.9(4)	O(3)−U−O(5)	151.0(3)
O(7)−U−O(2)	90.3(4)	O(3)−U−O(2)	72.2(4)
O(5)−U−O(2)	136.8 (4)	O(7)−U−O(1)	89.0(4)
O(9)−U−O(1)	91.4(4)	O(3)−U−O(1)	138.2(4)
O(5)−U−O(1)	70.7(4)	O(2)−U−O(1)	66.1(3)
O(7)−U−O(8)	88.5(4)	O(9)−U−O(8)	90.6(4)
O(3)−U−O(8)	75.8(4)	O(5)−U−O(8)	75.2(4)
O(2)−U−O(8)	148.1(4)	O(1)−U−O(8)	145.7(4)

[a] Symmetry transformations used to generate equivalent atoms: (#1) $-x+1, y, -z+1/2$.

Scheme 1. Canonical Forms of (A) dpp^- and (B) ma^-

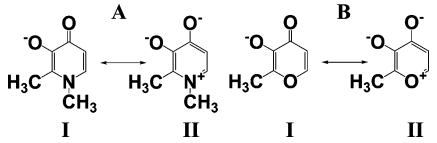

(30) Kuechle, W.; Dolg, M.; Stoll, H.; Preuss, H. *J. Chem. Phys.* **1994**, *100*, 7535.
(31) Bergner, A.; Dolg, M.; Kuechle, W.; Stoll, H.; Preuss, H. *Mol. Phys.* **1993**, *80*, 1431.
(32) Dunning, T. H., Jr.; Hay, P. J. *Modern Theoretical Chemistry*; Schaefer, H. F., Ed.; Plenum: New York, 1976; Vol. 3, p 1.
(33) Frisch, M. J.; Trucks, G. W.; Schlegel, H. B.; Scuseria, G. E.; Robb, M. A.; Cheeseman, J. R.; Montgomery, J. A., Jr.; Vreven, T.; Kudin, K. N.; Burant, J. C.; Millam, J. M.; Iyengar, S. S.; Tomasi, J.; Barone, V.; Mennucci, B.; Cossi, M.; Scalmani, G.; Rega, N.; Petersson, G. A.; Nakatsuji, H.; Hada, M.; Ehara, M.; Toyota, K.; Fukuda, R.; Hasegawa, J.; Ishida, M.; Nakajima, T.; Honda, Y.; Kitao, O.; Nakai, H.; Klene, M.; Li, X.; Knox, J. E.; Hratchian, H. P.; Cross, J. B.; Adamo, C.; Jaramillo, J.; Gomperts, R.; Stratmann, R. E.; Yazyev, O.; Austin, A. J.; Cammi, R.; Pomelli, C.; Ochterski, J. W.; Ayala, P. Y.; Morokuma, K.; Voth, G. A.; Salvador, P.; Dannenberg, J. J.; Zakrzewski, V. G.; Dapprich, S.; Daniels, A. D.; Strain, M. C.; Farkas, O.; Malick, D. K.; Rabuck, A. D.; Raghavachari, K.; Foresman, J. B.; Ortiz, J. V.; Cui, Q.; Baboul, A. G.; Clifford, S.; Cioslowski, J.; Stefanov, B. B.; Liu, G.; Liashenko, A.; Piskorz, P.; Komaromi, I.; Martin, R. L.; Fox, D. J.; Keith, T.; Al-Laham, M. A.; Peng, C. Y.; Nanayakkara, A.; Challacombe, M.; Gill, P. M. W.; Johnson, B.; Chen, W.; Wong, M. W.; Gonzalez, C.; Pople, J. A. *Gaussian 03*, revision A.1; Gaussian, Inc.: Pittsburgh, PA, 2003.

Table 3. Proton Chemical Shifts and Coupling Constants for **1** in DMSO-d_6 and **2** in DMSO-d_6 and CD_3CN with Numbering According to Chart 2

	chem shifts (ppm) [$^3J_{H(6)-H(5)}$ (Hz)]						
	DMSO-d_6/293 K		DMSO-d_6/323 K		CD_3CN/224 K for **2**[a]		
protons	free ligand	**1**	free ligand	**2**	**a**	**b**	**c**
6	8.02 [5.65]	8.43 [5.21]	7.53 [7.27]	7.67 [6.27]	7.85 [6.91]	7.67 [6.76]	7.83 [6.91]
5	6.33	6.92	6.08	6.34	7.22	6.68	7.22
7	2.24	2.65	2.28	2.61	2.47	2.64	2.44
8			3.63	3.87	3.82	3.82	3.82
OH	8.8		12.4[b]		12.3		12.0

[a] **a**−**c** are the three coordinated ligands (Chart 2). [b] In CD_3CN this peak appeared at 10.25 ppm.

mean bond distances in that molecule ($U-O_{oxo} = 2.432(5)$ Å and $U-O_{phenolate} = 2.350(5)$ Å) are comparable to those of complex **1.** Xu and Raymond have synthesized a series of tetradentate Me-2,3-HOPO ligands and their uranyl complexes.[4] These tetradentate ligands contain two Me-2,3-HOPO units linked with linear chain linkers. The X-ray structural analysis of these complexes showed the two HOPO units arranged around the equatorial plane of uranyl ion in the $\mathbf{C_{s2}}$ mode (Chart 1). The nonexistence of the $\mathbf{C_{s2}}$ structure for the bidentate hydroxy ketonate−uranyl complexes probably indicates that this coordination mode is the less stable one. The linkers of the tetradentate ligands have presumably forced the HOPOs to adopt the $\mathbf{C_{s2}}$ mode in these complexes.

The coordination environment of the uranium atom in **2** is a distorted pentagonal bipyramid with two oxo groups occupying the apical positions. The equatorial plane of **2** consists of an oxygen atom (from water) and four oxygen atoms originated from three ligands, two of which are single bonded and one is chelated (**P** coordination mode, Chart 1). The $d(C-O_{ketone})$ [C(8)−O(3), 1.278(16), and C(15)−O(5), 1.297(17) Å] of the two single-bonded Hdpp ligands in **2** were found significantly shorter (∼0.08 Å) than the $C-O_{hydroxy}$ bonds [C(9)−O(4), 1.366(16), and C(16)−O(6), 1.372(17) Å] indicating a double or partial double bond for the $C-O_{ketone}$ (type **I**). On the other hand, the indistinguishable C−O bond lengths [C(1)−O(1), 1.334(17), and C(2)−O(2), 1.316(18) Å] of the chelate dpp^- ligand in complex **2** support a catechol type **II** resonance form and increased aromaticity for the pyridinone ring. Remarkably, in **2**, U^{VI} forms very short bonds with the ketonic oxygen atoms of the two single-bonded Hdpp ligands [U−O(3), 2.273(9), and U−O(5), 2.281(9) Å] and long bonds with the oxygen atoms of the bidentate dpp^- [2.433(10) and 2.384(12) Å] for the U−O(1) and U−O(2) bonds, respectively. The −OH oxygen atoms of the single-bonded ligands are directed toward the oxygen atoms of the bidentate ligand (Figure 1), and the distances between them are 2.69(2) and 2.65(2) Å for O(2)−O(4) and O(1)−O(6), respectively. These O−O distances are shorter than either the sum of van der Vaals radii of the oxygen atoms (∼2.8 Å) or the distance of the water hydrogen-bonded oxygen atoms (2.76 Å) but are comparable to the hydrogen-bonded oxygen atoms of formic acid (2.67 Å), indicating the formation of strong hydrogen bonds. These strong hydrogen bonds probably provide the necessary energy for the stabilization of the **P** coordination mode over the **C** one and are responsible for the lengthening of $d(U-O_{chelate})$.

Chart 2. Numbering Arrangements of **1** and **2**

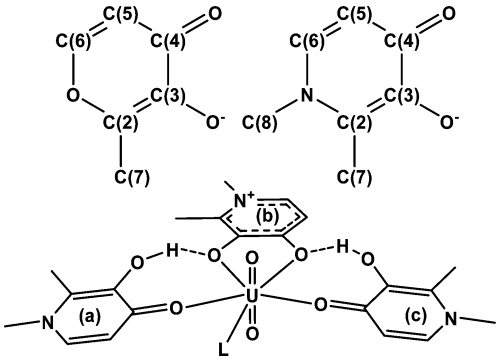

Assignments of ^{1}H NMR Spectra for 1 and 2 and ^{13}C NMR Spectra for 1. The solution structures were investigated by ^{1}H and ^{13}C NMR spectroscopy for complex **1** in DMSO-d_6 and by ^{1}H NMR spectroscopy for complex **2** in DMSO-d_6 and CD_3CN. Chemical shifts and assignments of the compounds and the free ligands in DMSO-d_6 and CD_3CN are listed in Table 3. The numbering of the ligands is shown in Chart 2.

The ^{1}H NMR spectrum of **1** in DMSO-d_6 at 293 K showed two doublets and one singlet peak assigned to the aromatic protons and the methyl group of the ligated ma^-, respectively. No peak was observed for the −OH protons, thus supporting complete deprotonation of the ligands in **1**. The ^{13}C NMR spectrum of **1** in DMSO-d_6 at 293 K showed only six resonances for the 12 carbon atoms of the two maltolate ligands. These experimental findings are in agreement with the symmetric structure of the compound found in the solid state by crystallography (Figure 1). The ^{1}H NMR spectrum of **2** in DMSO-d_6 at 291 K showed signals from ligated organic molecules and free ligand. On the basis of the integration of the spectra, it is evident that one out of the three ligands has been completely dissociated from the complex, and thus, free Hdpp ligand and at least two UO_2^{2+} species each containing two chelate dpp^- ligands (type **C** coordination mode) were generated.

Chart 1 shows the three possible geometrical configurations for the **C** coordination mode. The ^{1}H NMR spectrum of **2** gave peaks originating from two uranyl isomers, in a temperature range from 285 to 313 K. One isomer has been assigned to the complex containing two chelated dpp^- ligands in the $\mathbf{C_a}$ and the other in the $\mathbf{C_{s1}}$ coordination mode, based on the crystallographic data of the bis(hydroxy ketonate)−uranyl complexes. The protons of the coordinated ligands in the two isomers have similar chemical shifts, and the peaks are partially overlapped. With increase of the temperature,

these resonances coalesce above 45 °C resulting in two aromatic doublets (Figure S1) and two singlets in the aliphatic region, indicating a fast exchange reaction between the isomers at this temperature. In contrast, the ^{1}H and ^{13}C NMR spectra of **1** did not show any splitting or broadening of the peaks, even at 285 K, indicating that either only one isomer is present in DMSO-d_6 solution, presumably possessing the $\mathbf{C_{s1}}$ structure, or the isomers are exchanging fast even at this temperature. However, the latter is rather improbable. The similarities of the ligands and the structures between complexes **1** and **2** in DMSO-d_6 solution suggest that the exchange between the isomers of **1** is slow at this temperature with rates comparable to those of **2**. To examine if a UO_2^{2+} complex containing three coordinated bidentate ligands is present in the DMSO-d_6 solutions, free ligand was added in up to 20 times the concentration of uranium. However, the NMR spectra of these solutions did not show any formation of **P** type uranyl species.

The ^{1}H NMR spectrum of **2** in CD_3CN at 224 K gave peaks (Table 3) from three different coordinated ligands, indicating that **2** retains its integrity in CD_3CN solutions (**P** coordination mode). Furthermore, two peaks at 12.2 and 12.0 ppm have been assigned to the two hydroxide protons of the two single-bonded Hdpp ligands shifted downfield compared to the chemical shift of the free ligand's −OH proton (10.3 ppm) due to the formation of strong hydrogen bonds. The 2D ^{1}H COSY, the chemical shifts, and the $^3J_{H(6)-H(5)}$ coupling constants (Table 3) were used to distinguish the proton resonances of the chelate from the two single-bonded ligands. The ^3J values are very sensitive to small differences in the C−C bond lengths and are indicative for the bond alternation in cyclic π systems.[34] The $^3J_{H(6)-H(5)}$ of a and c rings are slightly larger than the $^3J_{H(6)-H(5)}$ of the chelated ring b ($\Delta(^3J) = 0.15$ Hz). For the six-membered aromatic systems, a 0.15 Hz difference represents a change of ∼0.02 of the Hückel π-bond order or 4×10^{-3} Å of the bond distance of C═C.[34a] Thus, the C(6)−C(5) bond distance of ring b should be only slightly shorter than the respective bond distances of either ring a or c as evidenced by the ^3J coupling constants. This prediction cannot be confirmed by the crystal structure because the error in the determination of these bond distances [1.38(2), 1.35(2), and 1.39(2) for the rings a−c, respectively] is larger than the differences observed by the NMR. The spectra of **2** in CD_3CN, at room temperature, gave broad peaks in the aromatic and aliphatic regions, thus indicating a dynamic process between the ligated ligands within the complex.

NMR Study of the Ligand Exchange of 2 in CD_3CN. The dynamic behavior of complex **2** was examined using variable-temperature and 2D ^{1}H EXSY NMR spectroscopy. The CD_3CN solution of **2** gave well-resolved resonances at 224 K, suggesting that the exchange between the three coordinated ligands is a slow process at this temperature, with respect to the NMR time scale. However, upon increase

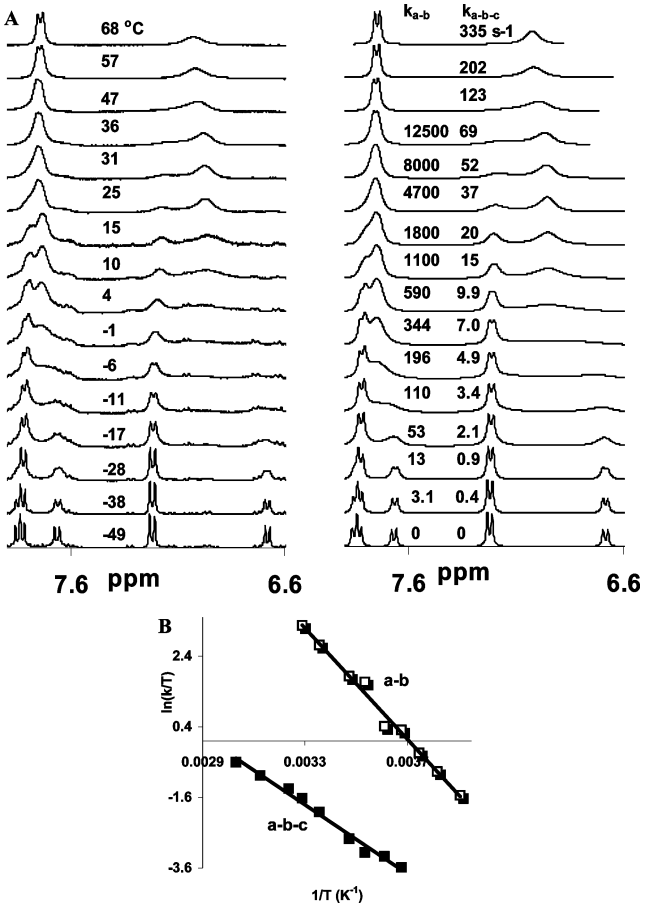

Figure 2. (A) VT ^{1}H NMR spectra (300 MHz) of **2** in CD_3CN (aromatic region), experimental spectra left and simulated spectra right (rates found from the Eyring plots used in the simulated spectra), and (B) Eyring plots for **a**−**b** and **a**−**b**−**c** exchanges, $\Delta H_{\mathbf{a}-\mathbf{b}}^{\ddagger} = 65 \pm 6$ kJ mol^{-1}, $\Delta S_{\mathbf{a}-\mathbf{b}}^{\ddagger} = 45 \pm 9$ J mol^{-1} K^{-1}, $\Delta H_{\mathbf{a}-\mathbf{b}-\mathbf{c}}^{\ddagger} = 41 \pm 4$ kJ mol^{-1}, and $\Delta S_{\mathbf{a}-\mathbf{b}-\mathbf{c}}^{\ddagger} = -78 \pm 5$ J K^{-1} mol^{-1}. Open and filled squares represent the rates for the **a**−**b** and **a**−**b**−**c** exchanges, respectively, calculated from the simulation of the experimental spectra.

Scheme 2. Different Hypothetical Exchange Mechanisms

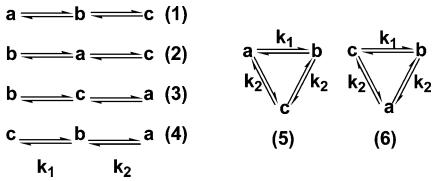

of the temperature at 10 °C the proton signals of the chelate dpp^- (**b**) coalesce with the respective proton signals of one of the single bonded bidentate ligands (process **a**−**b**), whereas at higher temperatures (∼68 °C) all signals coalesce (process **a**−**b**−**c**) to give one doublet and one broad aromatic peak and two singlets in the aliphatic region. Line-shape analysis of the aromatic region of the experimental spectra provided the respective calculated spectra and the rate constants for the two types of exchange (Figure 2A). The signals of the methyl protons [C(7)H_3] were not simulated because these peaks were partially overlapped by the broad water peak. Six different hypothetical exchange mechanisms, shown in Scheme 2, were used successively for the line fitting and mechanism 5 yielded the best fit. The rate constants were fitted as a function of $1/T$ according to the Eyring equation to obtain the activation parameters for both

(34) (a) Cooper, M. A.; Manatt, S. L. *J. Am. Chem. Soc.* **1970**, *92*, 4646. (b) Cooper, M. A.; Manatt, S. L. *J. Am. Chem. Soc.* **1969**, *91*, 6325. (c) Cooper, M. A.; Manatt, S. L. *J. Am. Chem. Soc.* **1970**, *92*, 1605. (d) Ammon, H. L.; Wheeler, G. L. *J. Am. Chem. Soc.* **1975**, *97*, 2326.

exchange processes (Figure 2B). The three-ligand exchange of complex **2** was confirmed by cross signals in the 2D ^{1}H EXSY experiments (Figure S2). However, the partial overlap of the proton peaks of ligands **a** and **c** prevented separation of the two exchange processes, **a**−**b** and **a**−**b**−**c**, by 2D ^{1}H EXSY spectroscopy.

Investigation on the Possible Mechanisms for the a−b and a−b−c Processes. The coalescence of ^{1}H NMR lines in the temperature range between −20 and 10 °C was attributed to an intramolecular exchange between the doubly and one singly bonded hydroxypyridone ligand (**a**−**b**) for the following reasons: (a) The line shape of the resonances and the exchange rates were not altered by adding small quantities of free Hdpp to the solution of **2**. (b) The intermolecular exchange reactions reported in the literature for UO_2^{2+} complexes with bidentate ligands, such as acetylacetone {k(25 °C) = 5.03 × 10^{-3} s^{-1}, $[UO_2(acac)_2(DMSO)]$}[35] and nonamethylimidophosphoramide {k(25 °C) = 3.4 × 10^{-3} s^{-1}, $[UO_2(NIPA)_3]^{2+}$},[19] exhibit much slower rates than the **a**−**b** [k(25 °C) = 4.7 × 10^3 s^{-1}].

Basically, the possible intramolecular mechanisms for the **a**−**b** exchange will involve (i) dissociation of the unidentate ligand, L, (ii) formation of U−O−C(**a**) bond and rupture of U−O−C(**b**) bond with proton transfer from ligand **a** to **b**, (iii) rupture of the hydrogen bond O(**b**)···H−O−C(**c**), rotation of **c** around the U−O═C(**c**) bond, and re-formation of the O(**a**)···H−O−C(**c**) hydrogen bond, and (iv) reattachment of the unidentate ligand. The relatively high activation enthalpy ($\Delta H_{\mathbf{a-b}}^{\ddagger}$ = 65 ± 6 kJ mol^{-1}) and the positive entropy ($\Delta S_{\mathbf{a-b}}^{\ddagger}$ = 45 ± 9 J mol^{-1} K^{-1}) indicate that either the dissociation of the unidentate ligand or the rupture of U−O−C(**b**) bond is the rate-determining step. To examine the former, variable-temperature ^{1}H NMR spectra of **2** in CD_3CN solutions containing DMSO 1−10 times the concentration of the complex were acquired (Figure S3, Supporting Information). ^{1}H NMR spectra showed that most of the complex **2** retains its structure in these solutions, with DMSO gradually replacing L, as was evidenced by the appearance of the peak at 3.15 ppm, assigned to the methyl protons of the coordinated DMSO. Structural and kinetic studies presented in the literature support that DMSO is stronger and more inert ligand than water for the uranyl moiety. In fact, the rate constants of the DMSO exchange in $[UO_2(DMSO)_5]^{2+}$ and that of the H_2O exchange in $[UO(H_2O)_5]^{2+}$ are 5.53 × 10^3 and 1.6 × 10^6 s^{-1}, respectively, at 25 °C.[36−39] The **a**−**b** exchange rate decreases drastically upon the substitution of H_2O with DMSO, thus supporting the dissociation of the monodentate ligand as the rate-determining step. Actually, the variable-temperature spectra of these solutions showed only the **a**−**b**−**c** exchange, indicating that the rate of **a**−**b** exchange for **2**, with L being

Scheme 3. Proposed Mechanisms of (A) **a**−**b** and (B), (C) **a**−**b**−**c** Exchange (M = UO_2^{2+})

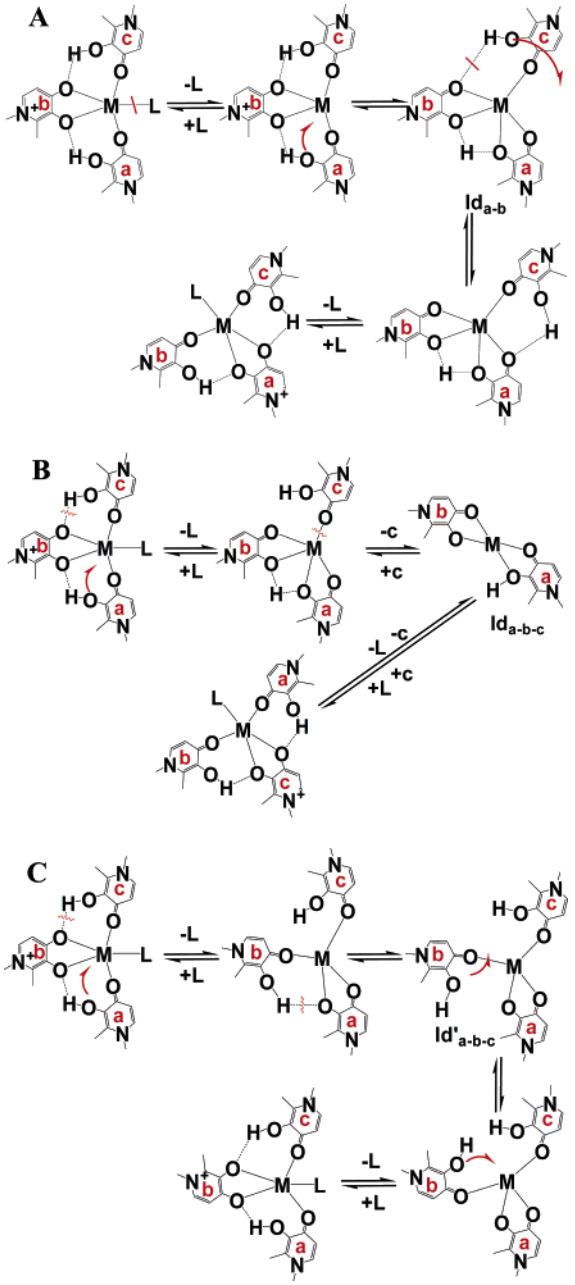

DMSO, is equal to or slower than the **a**−**b**−**c** exchange rate. Furthermore, the rate of **a**−**b** exchange [k(25 °C) = 4.7 × 10^3 s^{-1}] in CD_3CN is of order similar to the intermolecular exchange rates observed for unidentate ligands in related UO_2^{2+} complexes, such as $[UO_2(NIPA)_2(EtOH)]^{2+}$ [k(25 °C) = 1.0 × 10^4 s^{-1}] and $[UO_2(acac)_2(DMSO)]$ [k(25 °C) = 2.36 × 10^2 s^{-1}], supporting our assumption.[40,41] A possible mechanism that involves the detachment of L as the rate-determining step is illustrated in Scheme 3A. The phenolic oxygen of ligand **a** ligates the uranium atom forming the intermediate $\mathbf{Id}_{\mathbf{a-b}}$, which contains two chelate and one single bonded hydroxypyridone ligand. As evidenced

(35) Fukutomi, H.; Ikeda, Y. *Inorg. Chim. Acta* **1985**, *115*, 223.
(36) Ikeda, Y.; Tomiyasu, H.; H., F. *Bull. Res. Lab. Nucl. React. (Tokyo Inst. Technol.)* **1979**, *4*, 47.
(37) Ikeda, Y.; Tomiyasu, H.; Fukutomi, H. *Inorg. Chem.* **1984**, *23*, 3197.
(38) Farkas, I.; Banyai, I.; Szabo, Z.; Wahlgren, U.; Grenthe, I. *Inorg. Chem.* **2000**, *39*, 799.
(39) Vallet, V.; Wahlgren, U.; Schimmelpfennig, B.; Szabo, Z.; Grenthe, I. *J. Am. Chem. Soc* **2001**, *123*, 11999.
(40) Rodehuser, L.; Rubini, P. R.; Bokolo, K.; Delpuech, J.-J. *Inorg. Chem.* **1982**, *21*, 1061.
(41) Ikeda, Y.; Tomiyasu, H.; Fukutomi, H. *Bull. Chem. Soc. Jpn.* **1983**, *56*, 1060.

from the structures of the complexes **1** and **2** and the theoretical calculations, the two chelate ligands will ligate the uranium atom more strongly in the bis-chelate $\mathbf{Id_{a-b}}$ than the chelate ligand **b** in **2**. In addition, ligand **b** will possess a type **I** resonance form in the intermediate $\mathbf{Id_{a-b}}$. Consequently, the strength of the hydrogen bond between **c** and **b** becomes weaker in $\mathbf{Id_{a-b}}$ allowing **c** to rotate around U−O═C(**c**). Rotation 180° sets **c** in a position to form a hydrogen bond with **a**. The exchange reaction is completed by opening of the chelate ring of **b** and reattachment of L.

The second exchange (**a**−**b**−**c**) which gives coalescence of ^{1}H NMR lines in the temperature range between 30 and 70 °C may proceed through an intermolecular or an intramolecular mechanism.

Scheme 3B shows a possible intermolecular mechanism. The closure of ligand **a** is compatible with the negative value of the activation entropy ($\Delta S_{\mathbf{a-b-c}}^{\ddagger} = -78$ J K^{-1} mol^{-1}) and the low activation enthalpy ($\Delta H_{\mathbf{a-b-c}}^{\ddagger} = 41 \pm 4$ kJ mol^{-1}). As we have previously described, the closure of ligand **a** will reduce the strength of the hydrogen bond between the phenolic proton of **c** and the oxo atom of **b**. In a second step the single-bonded Hdpp, **c**, dissociates to give the six-coordinated intermediate $\mathbf{Id_{a-b-c}}$. The exchange reaction is completed by reattachment of ligand **c** from the side opposite to the dissociation side of **c**. Reattachment from the same side will exchange only **a** with **b** ligand.

An alternative intramolecular mechanism for the **a**−**b**−**c** exchange also compatible with the observed activation parameters is shown in Scheme 3C. The closure of the ring **a** is the first step of this mechanism. In a second step, the protonated chelate ring **b** opens ($\mathbf{Id'_{a-b-c}}$) and rotates around U═O−C(**b**) bond. Closure of **b** will result in the exchange between **c** and **a** and in combination with **a**−**b** in the exchange of all ligands.

To investigate if the intermolecular or the intramolecular mechanism is involved in this exchange, the ^{1}H NMR spectra of CD_3CN solution of **2** containing free Hdpp (the ratio of Hdpp to **2** was 0.1:1) at various temperatures were acquired. The broadness of the peaks due to the **a**−**b** exchange and partial decomposition of the complex did not allow quantification of the **a**−**b**−**c** exchange in the presence of free ligand. However, the peaks of the free Hdpp did coalesce with the resonances of the respective protons of the coordinated ligand at the same temperature range, indicating that the **a**−**b**−**c** is probably an intermolecular exchange. The intermolecular exchange reactions reported in the literature for UO_2^{2+} compounds containing bidentate ligands, such as $[UO_2(NIPA)_3]^{2+}$, $[UO_2(acac)_2(L)]$, and $[UO_2(ox)_2F]^{3-}$, have negative activation entropies (−38, ∼−90, and −74 J K^{-1} mol^{-1}, respectively) in line to the activation entropy of **a**−**b**−**c** ($\Delta S_{\mathbf{a-b-c}}^{\ddagger} = -78$ J K^{-1} mol^{-1}) supporting an intermolecular mechanism, although the possibility of an intramolecular mechanism cannot be totally excluded.[19,37,42,43]

Theoretical Calculations. To speed up the calculations, this theoretical study was undertaken using model ligands

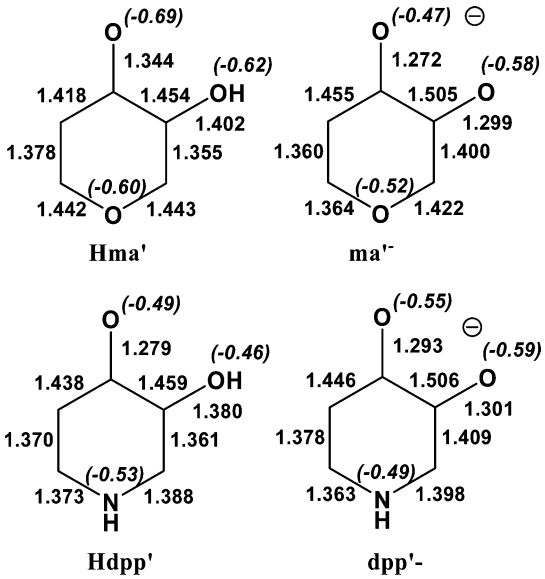

Figure 3. Calculated bond lengths and Mulliken charges of the nitrogen and oxygen atoms for the free and anionic forms of ligands Hma′, ma′$^-$, Hdpp′, and dpp′$^-$.

Hma′ and Hdpp′ in which the CH_3− groups of Hma and Hdpp have been replaced by H−. The molecular structures of the free ligands Hma′ and Hdpp′, as well as those of their anionic forms, ma′$^-$ and dpp′$^-$, have been optimized at the B3LYP level to explore their structure and electron-donor abilities. The bond lengths calculated and the Mulliken charges of the nitrogen and oxygen atoms are given in Figure 3. The bond lengths of the protonated ligands, Hma′ and Hdpp′, show a preference for a quinone form. In both ligands the negative charge is localized more on the oxo than on the phenolate oxygen. The bond length alternation in the anionic ligands supports a catecholate structure. The key differences between ma′$^-$ and dpp′$^-$ ligands is the almost equal C−O_{oxo} and C−$O_{phenolate}$ bond lengths and the equal charges of the oxo and phenolate oxygen atoms in the latter. Furthermore, the energy of the highest occupied σ and π donor orbitals of the ma′$^-$ ligand is higher than that of the corresponding orbitals of dpp′$^-$, supporting a higher electron-donor ability of the former.

The calculated bond lengths and angles of the model uranyl complex $[UO_2(ma')_2(H_2O)]$ (**1′a**) are given in Table 4. The optimized structure, shown in Figure 4, is symmetric ($\mathbf{C_{s1}}$ coordination mode), very close to a C_{2v} structure. As a result of the nonequal electron densities on the oxo and phenolate oxygen donor atoms in the ma′$^-$ ligand, the U−O_{oxo} and U−$O_{phenolate}$ bonds are nonequivalent (1.447 and 1.367 Å, respectively). There is a quite satisfactory agreement between the calculated structures of **1′a** and the experimental structure of **1**. Bond distances agree within 0.04 Å, while the largest deviation of bond angles appears to be about 4°. The greater discrepancy concerns the calculated longer U−O_{water} bond length, longer than the experimental value. The binding energy of each ma′$^-$ ligand, calculated as the energy difference between the complex and its fragments $[UO_2(H_2O)]^{2+}$ and $[(ma')_2]^{2-}$ in their nonrelaxed geometries, is 1062 kJ/mol, which gives a mean bond energy of 531 kJ/mol for

(42) Ikeda, Y.; Tomiyasu, H.; Fukutomi, H. *Inorg. Chem.* **1984**, *23*, 1356.
(43) Szabo, Z.; Grenthe, I. *Inorg. Chem.* **1998**, *37*, 6214.

Table 4. Selected Bond Distances (Å) and Bond Angles (deg) Calculated for Complexes **1′a** and **1′b**[a]

	1′a	**1′b**		**1′a**	**1′b**
U−O(1)	2.447	2.465	U−O(2)	2.367	2.367
U−O(4)	2.386	2.396	U−O(5)	1.772	1.774
U−O(1)$^{\#1}$	2.447	2.334	U−O(2)$^{\#1}$	2.367	2.472
U−O(5)$^{\#1}$	1.772	1.774			
O(1)$^{\#1}$−U−O(1)	76.7	76.9	O(2)$^{\#1}$−U−O(1)	141.6	142.0
O(2)−U−O(1)	65.2	65.3	O(4)−U−O(1)	141.6	141.9
O(5)$^{\#1}$−U−O(1)	89.2	92.9	O(2)$^{\#1}$−U−O(1)$^{\#1}$	65.2	65.1
O(2)−U−O(1)$^{\#1}$	141.6	142.2	O(4)−U−O(1)$^{\#1}$	141.6	141.2
O(5)−U−O(1)$^{\#1}$	89.2	92.0	O(5)$^{\#1}$−U−O(1)$^{\#1}$	91.0	92.0
O(2)−U−O(2)$^{\#1}$	153.1	152.7	O(4)−U−O(2)$^{\#1}$	76.6	76.1
O(5)−U−O(2)$^{\#1}$	91.0	88.5	O(5)$^{\#1}$−U−O(2)$^{\#1}$	88.4	88.5
O(4)−U−O(2)	76.6	76.6	O(5)−U−O(2)	88.4	90.0
O(5)$^{\#1}$−U−O(2)	91.0	88.5	O(5)−U−O(4)	88.6	86.8
O(5)$^{\#1}$−U−O(4)	88.6	86.8	O(5)$^{\#1}$−U−O(5)	177.3	173.4

[a] Numbering scheme as in Figure 4.

each U−O bond. An optimization with the model complex in a $\mathbf{C_a}$ coordination mode, resembling the structure found for $[UO_2(Me\text{-}2,3\text{-}HOPO)_2DMF]$,[4] gave a second minimum, **1′b**, as a nonsymmetric structure of C_s symmetry, located 69 kJ/mol higher than **1′a**.

The optimized structure for the complex $[UO_2(dpp')(Hdpp')_2(H_2O)]^+$, **2′**, is shown in Figure 4, whereas its calculated bond lengths and angles are given in Table 5. It corresponds to the experimental structure, with one bidentate, dpp′$^-$, and two single-bonded ligands, Hdpp′, coordinated through the oxo oxygen. The agreement in bond distances between theoretical and solid-state structures is satisfactory. The main difference between the structure determined by theory and that obtained from X-ray data is the conformation of the two monodentate ligands, which are planar but much more tilted out of the equatorial plane in the solid state than in the theory referring to the gas phase. The $U-O_{oxo}$ and $U-O_{phenolate}$ bonds of the bidentate ligand are almost equivalent (1.481 and 1.420 Å, respectively), whereas the $U-O_{oxo}$ bond of the single-bonded ligands is substantially shorter (1.338 Å). There are strong hydrogen bonds between the phenolate, O(2), or oxo, O(1), oxygen atoms of the bidentate ligands and the hydroxyl oxygen atoms of the monodentate ligand, O(4) and O(6), respectively. The corresponding O(2)···O(4) and O(6)···O(1)distances are 2.513 and 2.537 Å, respectively, with the O···H−O angle being 174° in both cases. Test calculations in which the hydroxyl groups have been rotated by 90° revealed that the two hydrogen bonds stabilize the complex by 238 kJ/mol. This value is the upper bound for the hydrogen bond energy as the structure without hydrogen bonds has not been fully optimized. The estimated mean binding energy for each of the four U−O bonds, calculated as the energy difference between the complex and its fragments $[UO_2(H_2O)]^{2+}$, [dpp′]$^-$, and [(Hdpp′)$_2$] in their nonrelaxed geometries, is 435 kJ/mol. This value is lower than the one found for complex **1′a**, quite in line with the predicted higher electron-donor ability of the ma′$^-$ ligand compared to dpp′$^-$.

Finally we have investigated the ring-closing process by formation of a $U-O_{phenol}$ by optimizing the complex $[UO_2(Hdpp')_2(dpp')]^+$ (**3**) after rotating the hydroxyl group of one of the monodentate ligands. The optimized structure

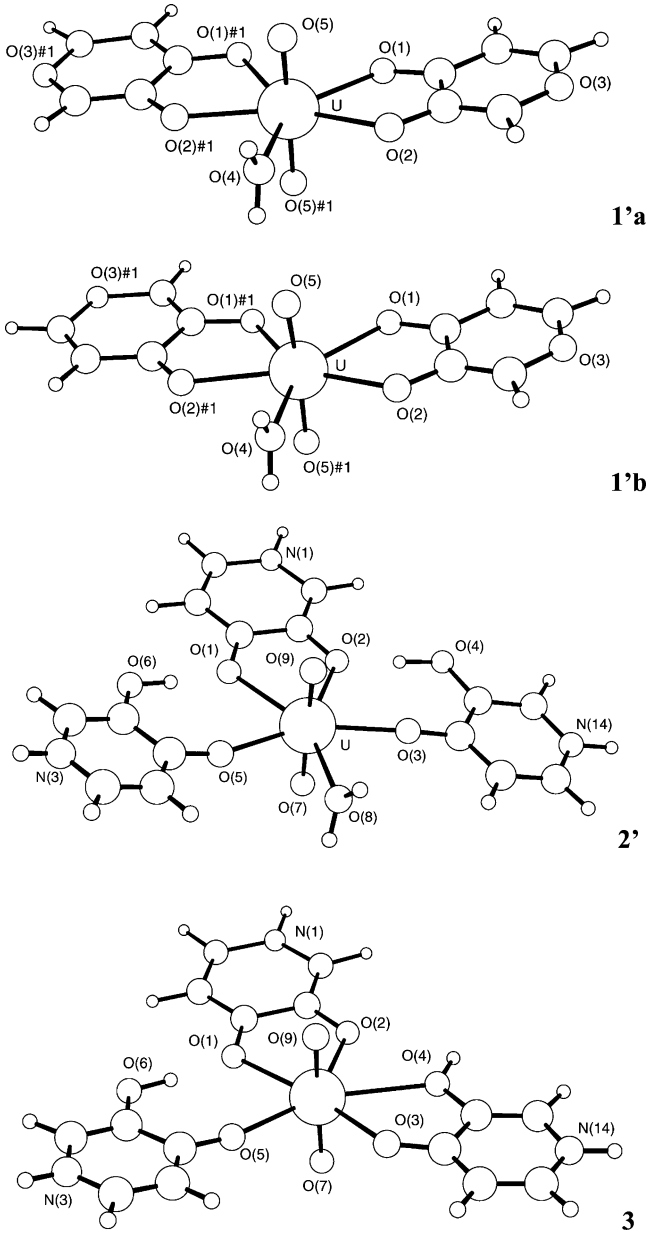

Figure 4. Optimized geometries of the complexes **1′a**, **1′b, 2′**, and **3**.

of **3** is shown in Figure 4, whereas its calculated bond lengths and angles are given in Table 5. In this structure one of the two Hdpp′ becomes a chelate ligand. The new $U-O(4)_{phenol}$ created has an elongated bond length of 2.514 Å. The ring closure results in the strengthening of the bond lengths of the chelate ligand dpp′$^-$, compared to those in the initial complex, particularly that of the $U-O(2)_{enolate}$ bond. The calculated electronic energy of the overall process

$$[UO_2(dpp')(Hdpp')_2(H_2O)]^+ \rightarrow [UO_2(dpp')(Hdpp')_2]^+ + H_2O$$

was found equal to −107 kJ/mol. Such a large reaction energy would be reflected in a large activation energy for the ring opening/ring closure reactions. Vallet et al.[44] have

(44) Vallet, V.; Wahlgren, U.; Grenthe, I. *J. Am. Chem. Soc.* **2003**, *125*, 14941.

Table 5. Selected Bond Distances (Å) and Bond Angles (deg) Calculated for Complexes **2′** and **3**[a]

	2′	**3**		**2′**	**3**
U−O(1)	2.481	2.439	U−O(2)	2.420	2.363
U−O(3)	2.338	2.347	U−O(5)	2.338	2.298
U−O(7)	1.767	1.758	U−O(8)	2.512	
U−O(9)	1.767	1.771	U−O(4)		2.514
O(7)−U−O(9)	176.1	174.6	O(7)−U−O(3)	89.1	88.3
O(9)−U−O(3)	90.61	86.6	O(7)−U−O(5)	89.5	88.6
O(9)−U−O(5)	88.9	90.2	O(3)−U−O(5)	151.0	97.3
O(7)−U−O(2)	91.5	91.7	O(3)−U−O(2)	73.0	122.4
O(5)−U−O(2)	136.0	140.2	O(7)−U−O(1)	92.8	91.6
O(9)−U−O(1)	90.0	93.1	O(3)−U−O(1)	136.8	171.1
O(5)−U−O(1)	72.1	73.7	O(2)−U−O(1)	63.9	66.5
O(7)−U−O(8)	87.2		O(9)−U−O(8)	88.9	
O(3)−U−O(8)	74.4		O(5)−U−O(8)	76.6	
O(2)−U−O(8)	147.4		O(1)−U−O(8)	148.7	
O(9)−U−O(4)		86.5	O(4)−U−O(2)		62.4
O(7)−U−O(4)		92.6	O(4)−U−O(5)		157.0
O(4)−U−O(1)		128.8	O(4)−U−O(3)		60.1

[a] Numbering scheme as in Figure 4.

shown that in the case of uranyl oxalate complexes the thermodynamic barriers are much lower in water-assisted reactions. Thus, this transformation could be accessible in solution.

Conclusions. Two novel uranyl−hydroxy ketone complexes **1** and **2** were crystallized from aqueous solution. The structure of **2** revealed a novel coordination mode (**P**) for the hydroxy ketonate ligands. Strongly coordinating solvents, such as DMSO, appeared to favor the **C** coordination mode over **P**, as evidenced by ^{1}H NMR studies. ^{1}H NMR spectra of **2** in CD_3CN showed that the complex preserved the **P** coordination mode after substitution of the H_2O unidentate ligand with DMSO, indicating that the type of the unidentate ligand did not influence the coordination mode of the bidentate ligands on uranyl. Solvation effects are probably responsible for the preference for the **C** structure in DMSO solution. The $\mathbf{C_{s1}} > \mathbf{C_a} > \mathbf{C_{s2}}$ stability order was predicted for the three possible isomers of **C** structure UO_2^{2+}-hydroxy ketonate complexes, based on crystallographic and ^{1}H NMR data. Theoretical calculations confirmed that $\mathbf{C_{s1}}$ is more stable than $\mathbf{C_a}$. On the basis of the solid and solution structural data and the DFT calculations, the stabilization of the **P** coordination mode of the ligands in complex **2** is attributed to the strong hydrogen bonds between the two single bonded Hdpp and the chelate dpp^-, as well as to the catecholate resonance form of the chelate dpp^-. The VT ^{1}H NMR studies demonstrated that the coordinated ligands in compound **2** are involved in two exchange processes: a fast intramolecular exchange between ligands **a** and **b** and a slower exchange, possibly intermolecular, among **a**−**c**. The calculated activation parameters and the decrease of the exchange rate upon replacement of the H_2O unidentate ligand by DMSO led us to propose the dissociation of the unidentate ligand and formation of an intermediate, containing two chelate and one single-bonded hydroxy ketonates, as the possible mechanism for the **a**−**b** process. The theoretical calculation also agrees with the proposed mechanism.

Supporting Information Available: Figure S1, variable-temperature spectra (aromatic region) of 20 mM **2** in DMSO-d_6, Figure S2, 2D ^{1}H EXSY NMR spectra of **2** in CD_3CN at −25 °C in the aromatic region, with mixing time $t_m = 200$ ms, Figure S3, variable-temperature spectra (aromatic region) of 20 mM **2** and 100 mM DMSO in CD_3CN, and crystallographic data in CIF format for complexes **1** and **2**. This material is available free of charge via the Internet at http://pubs.acs.org.

IC049167+